



Synthesis of a two-part geopolymer from red mud and silica fume

Arup Kumar MANDAL^{1,*}

¹ Department of Metallurgical and Materials Engineering, National Institute of Technology, Mahatma Gandhi Avenue, Durgapur, 713209, West Bengal, India

*Corresponding author e-mail: arup.mandal@mme.nitdgp.ac.in

Received date:

23 December 2020

Revised date:

13 April 2021

Accepted date:

16 April 2021

Keywords:

Red mud;
Silica fume;
Two-part geopolymer;
Waste materials

Abstract

In this present study, the development of a two-part geopolymer from waste red mud (RM) and silica fume (SF) by alkali activator is examined. The influence of silica fume addition, alkali concentration, curing duration are studied. The compressive strength of geopolymers has been achieved 0.8 MPa to 8 MPa with varying different compositions and synthesis parameters. The optimum RM/SF ratio is 60/40, the optimum solid/solution ratio is 1.8 g·mL⁻¹ or 2 g·mL⁻¹, and the optimum Na₂SiO₃/NaOH ratio is 0.5 day for 28 days curing time. The incorporation of iron in the geopolymer matrix contributes to geopolymerization. The study suggests that the produced geopolymer can be used as cementitious materials for making pavement and other valuable constructional materials. This procedure will be environment friendly and cheaper also.

1. Introduction

Many research has been carried out to examine the possibility of a geopolymer in construction applications. Nowadays, geopolymer studies are providing attention because of their potential to be used as a cost-effective substitute to inorganic cement, the organic polymer in different applications like aircraft, military applications [1,2], for preparing high technology ceramic, thermal insulating foams, fireproof building materials [3-7], for making protective coatings and adhesive [8-9], etc.

As an alternative to portland cement, geopolymers are emerging as the binder of structural concrete due to their energy efficiency, durability, and eco-friendly production method [10]. The production process of ordinary portland cement (OPC) contributes significantly to greenhouse gases than geopolymers, producing moderately low CO₂ emissions [11]. Geopolymers promises to have excellent potential for greenness and durability. The raw materials for geopolymers' production are alumina-silica containing waste materials from different industries. Synthesizing of geopolymer from various raw materials can be used with less restriction on particle size, purity, and composition. A variety of aluminosilicate materials are used to produce geopolymers like metakaolin, fly ash, bottom ash, blast furnace slag etc. [12-16]. Curing for geopolymer production is requires very low-temperature thermal treatment, generally from ambient to below 100°C [17]. The simplicity in geopolymer production from a range of aluminosilicate sources comprising waste materials offers a challenging task to characterize the precursor material fundamentally.

A significant amount of waste is produced by the 'Bayer' process to extract alumina from bauxite ore as a by-product. Subject to bauxite ore quality, the red mud generation varies from 55% to 65% of the

treated bauxite [18]. It is assessed that ~100 million tones of red mud are produced yearly throughout the world, in which India is producing ~5 million tones [19-21]. Red mud is a highly alkaline slurry containing a large NaOH solution dissolved in water used to extract silicates and alumina during digestion. Due to high alkalinity, it leaches and contaminates the groundwater and creates environmental problems. Thus, disposal and treatment of red mud are significant problems in aluminium plants. Different researches done on the effective utilization of red mud, but an extensively recognized technology for employing red mud recycling are not available [15,22-26].

Silica fume is very fine, a by-product generated from ferrosilicon or silicon production plant. It contains mainly non-crystalline (amorphous) silicon dioxide (SiO₂). Its fine particles, large surface area, and higher amount of amorphous SiO₂ content are very reactive pozzolana. Concrete having silica fume can make it very high strength and durable also [27]. The addition of silica fume in fly ash geopolymer, improves the mechanical and durable properties of the concrete [28]. Conventionally geopolymer is produced by sodium-based alkali solution containing sodium hydroxide and sodium silicate. Silica fume are widely used to increase the geopolymer's active silica content, where fewer silica materials are used for geopolymerization [29]. The red mud is also less silica-containing materials; hence one-part geopolymer preparation from red mud is impossible. To get adequate strength, it requires an additional silica source for geopolymerization. Silica sand, fly ash, is generally reported in the literature for making the geopolymer of red mud [15,30]. The combined utilization of fly ash and red mud for making constructional products is growing fast. The high strength geopolymer production with highly alkali solution, combined with red mud and bauxite, was also reported without adding strength promoting components [31]. Still, silica fume as strength-

promoting components in red mud for making a two-part geopolymer are not yet reported in the literature [15,32-34].

Red mud contains silica and alumina in low quantity compared to other aluminosilicate materials. Hence, it must be used with different materials; thus, its popularity in geopolymerization is relatively less. It can be used by the use of silica fume, which contain very high fine reactive silica. For such benefits, the present work aims to prepare a two-part geopolymer by the suitable blending of red mud and silica fume with an alkali activator.

2. Experimental

2.1 Raw materials and their characterization

The red mud used for geopolymer synthesis was procured from Hindalco Industries Limited, Renukoot, Uttar Pradesh. Silica fume was procured from an alloy company in Nagpur, Maharashtra. Laboratory grade (99%), sodium hydroxide pallets manufactured by LOBA CHEMIE, was used with 40 g as molecular weight, and laboratory-grade (97%) anhydrous sodium-meta-silicate powder was used. The molecular weight of sodium metasilicate is 122.08 g. The chemical composition of all the raw materials is shown in Table 1.

The particle size analysis is shown in Figure 1 and Table 2 red mud contains mainly silt size particles. The plasticity index lies between 7-17, and it can be classified as silt with intermediate compressibility (MI) as per the Indian Soil Classification System. A large amount of clayey content in red mud enhances the plasticity, which favors the brick formation by molding. The particles of silica fume are ultra-fine. All particles are below 5 μm in size.

The XRD analysis of the raw materials shown in Figure 2. Bauxite is a combination of different mineralogical forms of aluminium hydroxide like gibbsite, diaspore, boehmite etc., along with hematite. Therefore, red mud contains various aluminum hydroxides, hematite, goethite, cancrinite, etc [24]. Cancrinite is a zeolite group of minerals that has the typical generalized formula $(Na, Ca, K)_{7-8}[(Si, Al)_{12}O_{24}(CO_3, OH)_2 \cdot 2-3H_2O]$ [35]. Some alumina and silica are present as corundum and quartz, respectively, as a separate phase. The silica fume contain almost 100% amorphous silica phase, evidenced by a broad hump between 2 theta 20° to 30° [10,36,37].

Table 1. Chemical composition of raw material (wt%).

Compound	Red mud	Silica fume
Al ₂ O ₃	31.11	0.616
SiO ₂	25.78	91.30
Fe ₂ O ₃	24.96	1.47
TiO ₂	7.31	-
Na ₂ O	6.41	0.082
P ₂ O ₅	0.39	0.171
ZrO ₂	0.649	
SO ₃	0.613	3.13
CaO	1.68	0.38
V ₂ O ₅	0.266	
MgO	-	1.29
K ₂ O	-	0.653

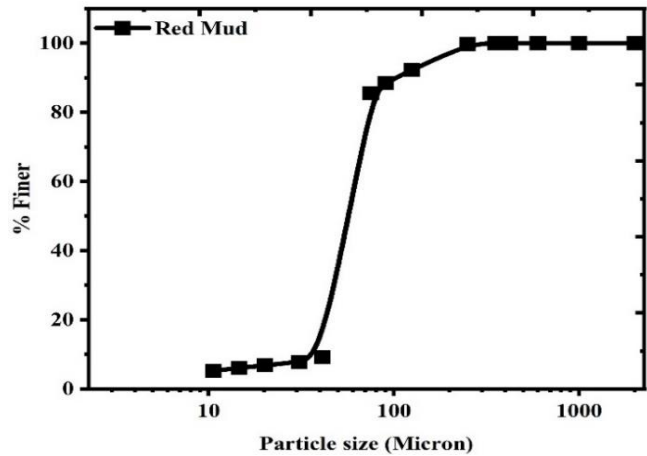


Figure 1. Particle size of the red mud.

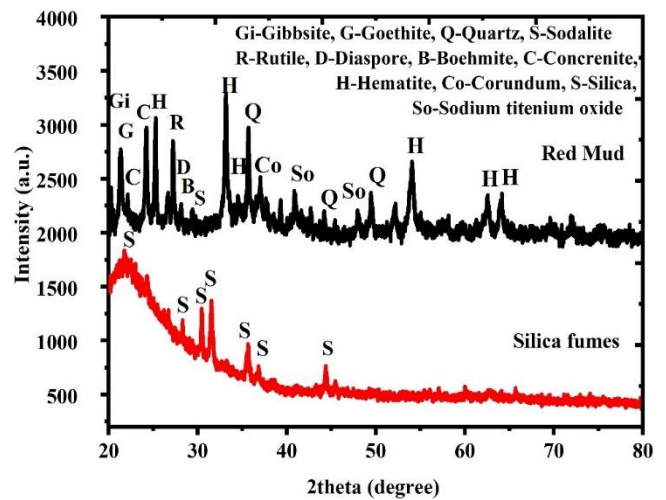


Figure 2. XRD analysis of silica fume and red mud.

Table 2. The grain size analysis of red mud.

Parameters	Red mud
Gravel (%)	0
Sand (%)	14.5
Silt and clay (%)	85.5
D ₁₀ mm	0.041
D ₃₀ mm	0.05
D ₆₀ mm	0.061
Coefficient of uniformity (C _u)	1.48
Coefficient of curvature (C _c)	1
Liquid limit (%)	45.5
Plastic limit (%)	32.3
Plasticity index (PI)	13.2
IS classification	MI

2.2 Methods

The dried red mud was pulverized to powder finer than 250 μm to get a larger surface area for facilitating geopolymerization reaction. After impurities removal, silica fume are air-dried mixed thoroughly

in a tray at fixed ratios as required blending in a dry condition, as shown in Table 3. The activator solution comprised of NaOH and Na₂SiO₃ was kept for 24 h before its usage. The mixture was then blended with different waste materials for 10 min to 15 min to allow adequate reaction between solution and solids to better dissolve silica and alumina with the required amount of water. The blending resulted in a geopolymer precursor paste. The paste was filled in cylindrical molds with a 38 mm diameter and 150 mm length. The filled molds were placed on a vibrating table for 5 min to remove the air bubble entrapped inside the paste. The molds were kept in the ambient environment for 4 days to allow initial curing; the specimens were then de-molded, followed by prolonged curing in ambient and exposed conditions. De-molded samples were first cut into the standard size of 38 mm × 76 mm. Samples were also kept in the oven, wrapped in poly-bags at 80°C to 85°C. Poly-bags prevented the excessive loss of curing fluid in the oven.

Previous work has reported that the amorphous aluminosilicate having a three-dimensional network and also cementation properties are the reason for strength development [38]. Devedovits *et al.* suggested a geopolymer's synthesis to make a strong product at a composition range M₂O/SiO₂=0.2-0.48; SiO₂/Al₂O₃=3.3-4.5; M₂O/Al₂O₃=0.8-1.6 and H₂O/M₂O=10-25 where M is alkali metals (Na, Ca etc). A lot of researchers also got similar results [23,31,39-43]. For the above-said reasons, experiments were designed to decrease the number of tests.

For making the red mud silica fume, bricks with sodium hydroxide alkali solution RM/SF ratios (i.e., 80/20, 70/30, 60/40, 50/50, 40/60) were selected at a fixed solid/solution ratio of 2 g·mL⁻¹.

The RM/SF ratio of 60/40 was chosen for determining the optimum solid/solution ratio and the curing duration. The solid/solution ratio was varied as (1.5, 1.8, 2.0, 2.5, and 2.8) g·mL⁻¹ and the samples were tested at a curing period of 5, 7, 14, 21, 28 days. The purpose of selecting the different RM/SF ratios is to examine the optimum quantity of red mud used for geopolymer synthesis to use the red mud waste as much as possible. Red mud previously contains a substantial amount of sodium hydroxide; still, 4 M concentration was used as the geopolymerization reaction did not occur at zero NaOH concentration. The samples after 7, 14, 21, and 28 days curing period were tested (Table 3).

2.3 Testing

The strength value of cured geopolymer sample was determined by unconfined compression strength. The two ends were polished

using sandpaper to get smoother sample surfaces. X-ray diffraction (XRD) characterized the red mud compositions, silica fume, and 28 day-cured geopolymers were characterized by X-ray diffraction (XRD). The microstructure of the geopolymers was examined using SEM. Samples for XRD and SEM analysis were prepared from the failed compression test specimens. The fracture surface was observed under SEM to see the internal structure, and the powder sample was used for XRD analysis to determine the different phases present inside the geopolymer.

3. Results and discussion

3.1 Red mud and silica fume bricks

3.1.1 Curing duration in ambient exposure conditions

The optimum curing period of red mud – silica fume geopolymer was found to within 14 days to 21 days. The maximum UCS value reached within 21 days and was 4.29 MPa. However, the specimen cured for 28 days showed an increase in modulus of elasticity and brittleness. Figure 3 shows the failure pattern of geopolymers at three durations 7, 14, and 28 days. The 7-day failure shows a ductile failure, while the 28-day failure was brittle. With the increase in the curing period, the ductility of samples decreased, and the compressive strength increased. There was an enormous increase in UCS values from 7 days to 14 days and only a slight increase from 14 days to 28 days, the same being the case of decreased ductility. Figure 4 shows the variation of UCS values of geopolymer with the curing duration.

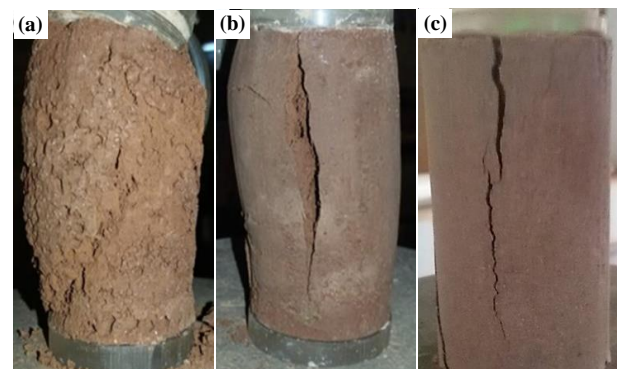


Figure 3. Failure pattern of red mud/silica fume (60/40) geopolymers (a) 7 days (b) 14 days (c) 28 days.

Table 3. Blending of different materials in dry condition.

Sample name	Red mud	Silica fume	SiO ₂ /Al ₂ O ₃	Na ₂ O/SiO ₂	Na ₂ O/Al ₂ O ₃
R80S20	80	20	1.91	0.49	0.93
R70S30	70	30	2.48	0.42	1.03
R60S40	60	40	3.22	0.36	1.17
R50S50	50	50	4.26	0.32	1.36
R40S60	40	60	5.78	0.28	1.62

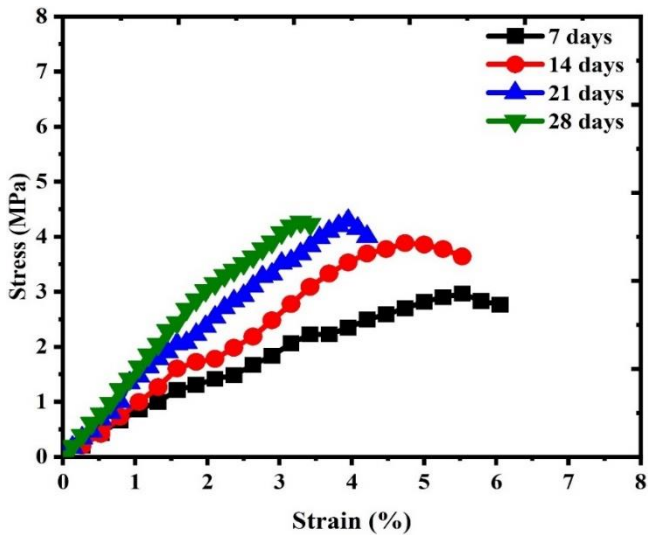


Figure 4. Stress-strain curves of RM/SF ratio of 60/40 for optimum curing duration in the ambient environment at a solid/solution ratio of 2 g·mL⁻¹.

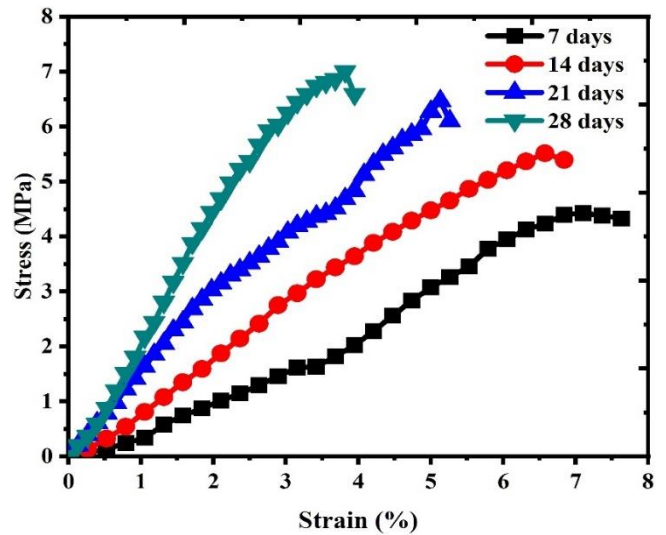


Figure 5. Stress-strain curves of RM/SF ratio of 60/40 for optimum curing duration at elevated temperature at a solid/solution ratio of 2 g·mL⁻¹.

3.1.2 Curing duration in oven

The stress-strain diagram of elevated temperature with various curing duration is shown in Figure 5. The curing temperature was set at 80°C to 85°C. The maximum UCS value was found to be 7 MPa at a 28-day curing duration. The variations in UCS values and ductility for curing duration were similar to ambient curing, the difference being the higher rate of increase of early strength. Also, the value of compressive strength was more significant than the value of ambient temperature cured samples. It showed brittle failure during the compressive strength test. It is due to the increasing the curing duration increases the hydrothermal products, responsible for strength development [44,45]. Compared to the ambient curing (as discussed in Section 3.1.1), curing in slightly increasing temperature, the rate of geopolymerization increases, resulting in more and quick strength development inside the product [46].

3.1.3 Variation of RM/SF ratio

As seen in the literature review, the increasing silica content would increase the UCS value and decrease the ductility. It was also confirmed by the results of this geopolymer also. Figure 6 shows the variation of stress-strain curves with the RM/SF ratio.

The maximum strength was found 6.53 MPa and 7.35 MPa for 14 days and 28 days cured samples, of samples having RM/SF ratio 60/40. With an increase in silica fume content, the geopolymer precursor showed higher resistance to flow. This increased resistance leads to the rise in several voids in the specimens, which may lead to premature failure of the specimen. Also, many uneven results were obtained while testing the samples with high silica fume content. Though the strength increases with an increase in silica content, geopolymers with high silica content deteriorate at the outer surface more. Hence the optimum ratio can be selected as 50/50.

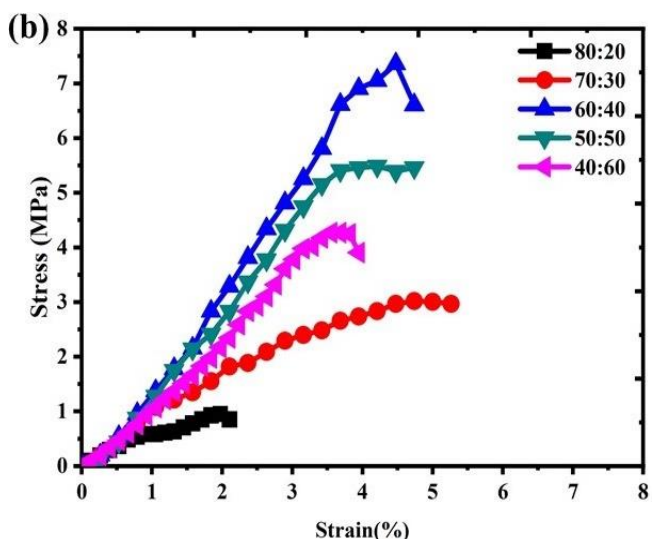
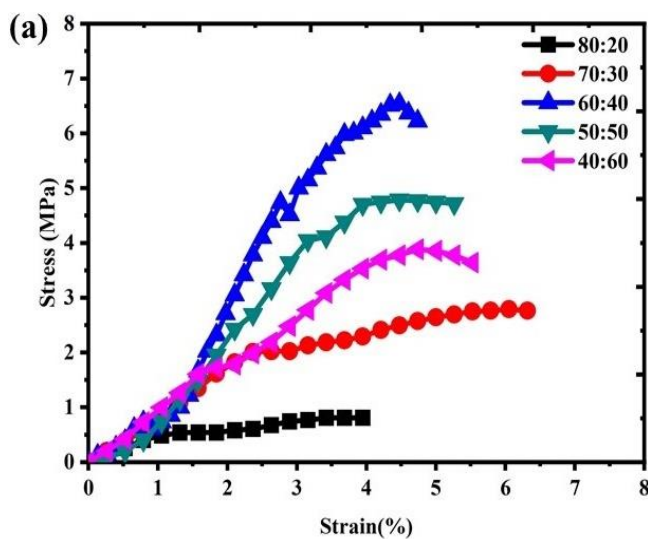


Figure 6. Stress-strain curves of different RM/SF ratio (a) 14-days (b) 28 days at a solid/solution ratio of 2 g·mL⁻¹.

3.1.4 Variation of solid/solution ratio

The solution comprises alkali activators and water. An increase in the amount of alkali activator may increase the dissolution of amorphous alumina and silica, but too much rise has been found to have adverse effects. When the ratio was decreased from 2 g·mL⁻¹ to 1.8 g·mL⁻¹, the performance of geopolymer upgraded, but with a further decrease to 1.5 g·mL⁻¹, the strength was drastically reduced. With more solution content, the density of the sample decreased. Also, there was a high amount of deterioration of the outer surface and shrinkage of samples.

When the ratio was increased to 2.5 from 2, both compressive strength and modulus of elasticity decreased, attributed to reduced activation and decreased silica content (from sodium silicate). However, the strength increased for the ratio 2.8, owing to a higher degree of solid compaction. Though the strength is high at this ratio, it can still not be selected as optimum due to great sample preparation difficulty. It took 40 min just to mix this sample due to the minimal solution (water content). It was challenging to obtain a uniformly mixed precursor paste. The paste obtained was of very little consistency. Hence the optimum ratio can be selected as 1.8 g·mL⁻¹ or 2 g·mL⁻¹, with both portraying nearly equal results. Figure 7 shows the variation of strengths with solid/solution ratio.

3.1.5 Variation of sodium silicate content (Na₂SiO₃/NaOH ratio)

The ratio was varied from 0 to 2. The optimum ratio has been found to be 0.5. Starting from 0, the modulus of elasticity was appreciable at this ratio, but the strength was lowest. Large surface cracks also appeared on the sample surface. At a ratio 0.5 the strength increased considerably. Further rate increase led to a decrease in strength and modulus of elasticity. The specimens with high ratios had greater consistency while paste preparation.

The specimens with ratio 1.5 and 2.0 were found to be ductile. The specimen with a ratio of 2.0 highly deteriorated, and efflorescence was seen on the surface due to unreacted sodium silicate presence. Figure 8 shows the variation of Na₂SiO₃/NaOH ratio of the compressive strength of the samples.

Figure 9 shows the failure pattern of geopolymers with Na₂SiO₃/NaOH ratio (a) 2 (b) 1. The degree of surface deterioration is evident in the figure with Na₂SiO₃/NaOH ratio of 2.0. The geopolymer with the lower content of alkali activator produces less geopolymer, resulting less strength [47].

3.4 XRD analysis

Figure 10 shows the XRD pattern of red mud, silica fume, and geopolymer. XRD graph of silica fume shows high broad hump 10° to 40° (2θ) centered about 22°. The broad hump denotes the amorphous content present in silica fume, which confirms its reactive nature. X-ray diffraction patterns before and after alkali activation are similar, and both contain a mixture of crystalline and amorphous phases. Various crystalline peaks of quartz, hematite aluminium hydroxide phases are present in geopolymer also, but the crystalline phases' intensity decreases considerably in geopolymer. Iron in geopolymer is present as Fe(II) in olivine (Mg_{0.9}Fe_{0.1})₂SiO₄. Other phases are present as

sodium-based Anorthite (Ca,Na)(Si,Al)₄O₈ and sodium aluminosilicate hydroxide hydrate Na₈(AlSiO₄)₆(OH)₂·4H₂O. The presence of such phases suggests that some dissolved red mud particles form crystalline phases. But significant reaction products are amorphous [48].

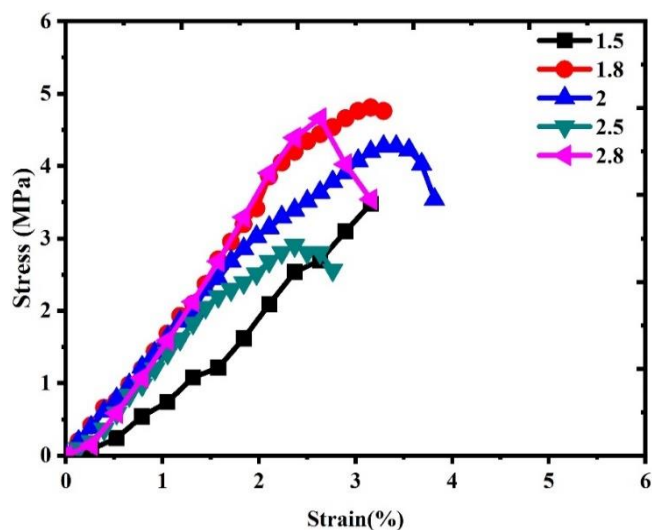


Figure 7. Stress-Strain curves RM/SF ratio of 60/40 for optimum solid/solution ratio.

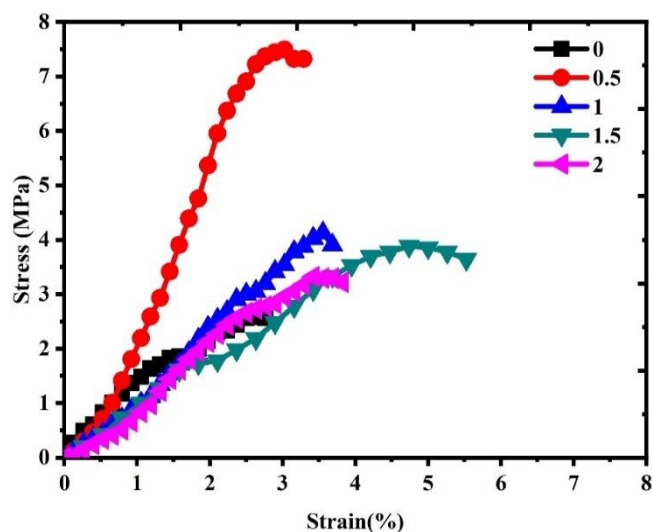


Figure 8. Stress-Strain curves of RM/SF ratio of 60/40 for optimum Na₂SiO₃/NaOH ratio at a solid/solution ratio of 2 g·mL⁻¹.

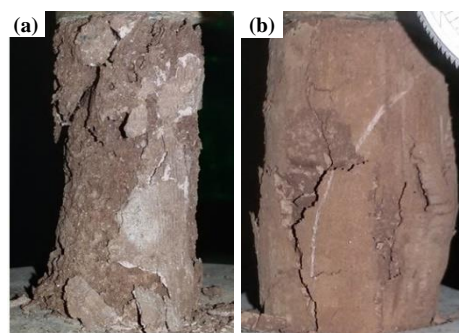


Figure 9. Failure patterns of geopolymers RM/SF ratio of 60/40 with Na₂SiO₃/NaOH ratio (a) 2 (b) 1.

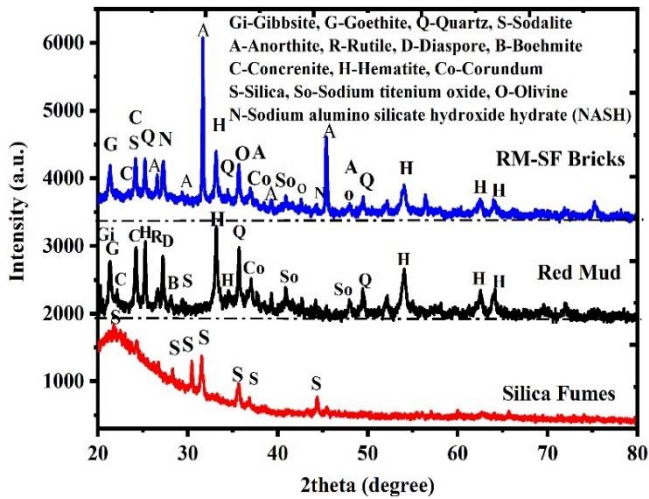


Figure 10. XRD graph of red mud silica fume geopolymer.

The XRD peak of geopolymer shows the reduced peak intensities of the crystalline material present in red mud. It confirms that the crystalline phases are not reactive and do not take part in geopolymer reaction. A broad hump is also seen in the XRD graph of a geopolymer. There is a shift in the center of that broad hump centered around 27° compared to the center of the broad hump of silica fume. This shift and the broad hump is the characteristic curve for all geopolymers and is independent of the type of source materials [3,49,50].

Due to presence of iron in red mud, all products' elemental composition shows a significant amount of iron. The high amount

of Fe in geopolymer gel occurred by substituting the Al [37,48]. Davidovits *et al.* suggested that, after alkali activation a change of iron environment from octahedral to the tetrahedral site can be possible when incorporated into a geopolymer framework. During the alkali activation, iron's behavior relies on its starting materials' mineralogical and chemical states. Therefore, after alkali activation, Fe-bearing minerals' peak intensity decreases significantly, indicating more iron in the glassy phase, which participates in polymerization reaction. Iron incorporation inside the Ferro-silicate matrix geopolymer is also reported by several authors [41]. It means incorporating iron ions in the geopolymer matrix helps increase the geopolymerization reaction and ultimately responsible for its strength increment.

3.5 SEM Images

The red mud morphology comprises irregular layered aggregates. The SEM image of silica fume shows ultrafine spherical particles packed loosely. The geopolymer SEM shows large aggregates with irregular and angular edges. It may be inferred from the image that red mud and silica fume have combined chemically to form large particles. Generally, a geopolymer is characterized by platy films, as seen in the picture. The SEM image of geopolymer at lower magnification shows certain loose microspheres showing the presence of unreacted particles. Figure 11 shows the SEM images of red mud, silica fume, and geopolymer. The bulk density of geopolymer has a greater effect on the formation of pores in geopolymer samples. These results affected the microstructure and compressive strength and agreed with the finding derived by other researchers also [51-52].

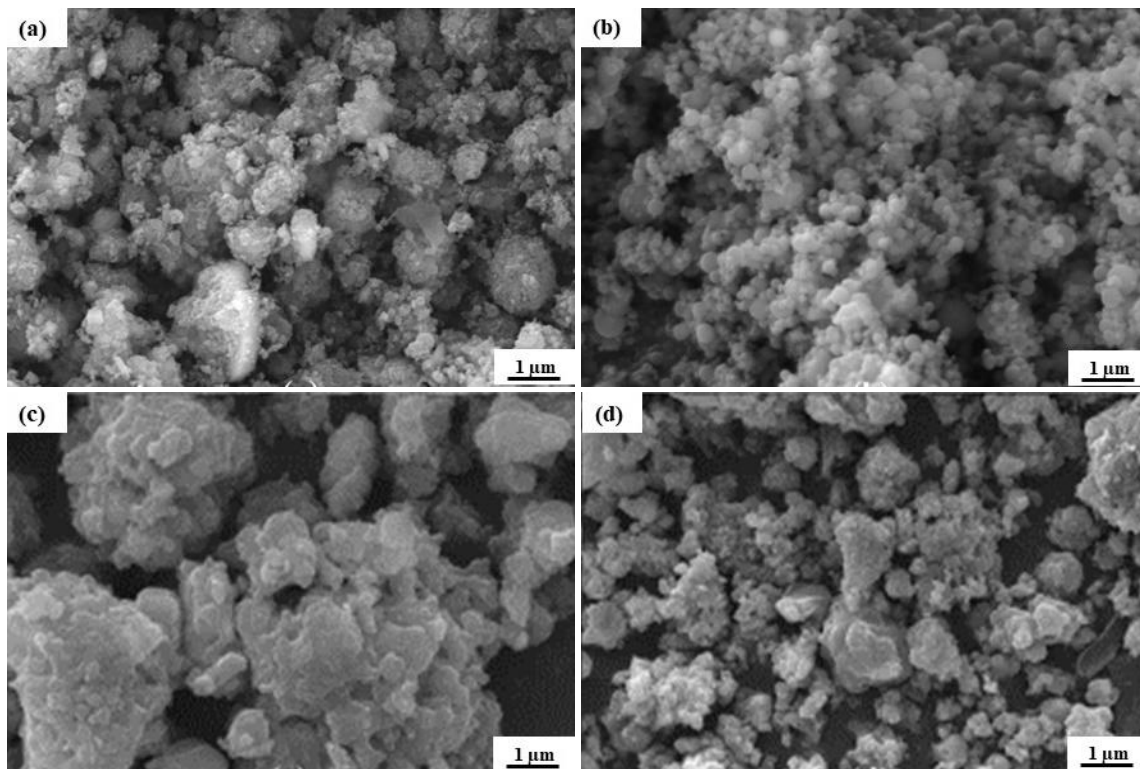


Figure 11. SEM images of (a) red mud (b) silica fume (c) and (d) geopolymer.

4. Conclusions

The results demonstrated that all the above-listed parameters influence the compressive strength of the geopolymer. For the studied range of compositions and synthesis parameter variations, geopolymers' compressive strength was found in the range of 0.8 MPa to 8 MPa. The optimum curing duration of geopolymers can be concluded as 28 days, depending on the amount of silica content. The stiffness increases with an increase in curing duration, and the strength also stabilizes with time. High-temperature curing increases the compressive strength and decreases the curing time. The deterioration of geopolymers' outer surface is also negligible during elevated temperature curing. Curing at ambient and exposed conditions causes surface deterioration and efflorescence due to alkali presence. The optimum RM/SF ratio was 60/40, the optimum solid/solution ratio was 1.8 g·mL⁻¹ or 2 g·mL⁻¹, and the optimum Na₂SiO₃/NaOH ratio was 0.5. With the increase in red mud content, the strength of geopolymer decreases. Incorporation of iron in the geopolymer matrix and contribute to the geopolymerization. The addition of solid/solution ratio decreases the strength of the geopolymer and vice versa. The amorphous silica fume increase the dissolution behavior of silica species resulting increase in strength. This study demonstrates that geopolymers can be used as cementitious materials, which can be used as a making-of pavement, and other useful applications. It can be considered as an environment friendly product.

Acknowledgements

The author is very grateful to the Department of Metallurgical Engineering, IIT(BHU), Varanasi, for allowing me to perform characterization work.

References

- [1] R. E. Lyon, P. N. Balaguru, A. Foden, U. Sorathia, J. Davidovits, and M. Davidovics, "Fire-resistant aluminosilicate composites," *Fire and Materials* vol. 21, pp. 67-73, 1997.
- [2] D. Hambling, "Cool Under Pressure: Geopolymers Offer Diverse Structural Benefits," *Defense Technology International*, Washington, DC. 2009, pp. 42.
- [3] J. Davidovits, and M. Davidovics, "Geopolymer: ultra-high temperature tooling material for the manufacture of advanced composites", in *the 36th International SAMPE Symposium, SAMPE 1991, San Diego, USA*, vol. 36(2), pp. 1939-1949, 1991.
- [4] V. Vaou, and D. Pnias, "Thermal insulating foamy geopolymers from perlite," *Minerals Engineering*, vol. 23(14), pp. 1146-1151, 2010.
- [5] K. Sakkas, S. Kapelari, D. Pnias, P. Nomikos, and A. Sofianos, "Fire resistant k-based metakaolin geopolymer for passive fire protection of concrete tunnel linings," *Open Access Library Journal*, vol. 1(6), pp. 1-9, 2014.
- [6] P. Puksisuwan, P. Laoratanakul, and B. Cherdhirunkorn, "Utilization of aluminium dross as a main raw material for synthesis of geopolymer," *Journal of Metals, Materials and Minerals*, vol. 27, pp. 35-42, 2017.
- [7] S. Prasanphan, A. Wannagon, and T. Kobayashi, "Microstructure evolution and mechanical properties of calcined kaolin processing waste-based geopolymers in the presence of different alkali activator content by pressing and casting," *Journal of Metals, Materials and Minerals*, vol. 30, pp. 121-132, 2020.
- [8] A. M. A. B. Mohd, L. Jamaludin, K. Hussin, M. Binhussain, C. M. R. Ghazali, and A. M. Izzat, "Study on fly ash based geopolymer for coating applications," *Advanced Materials Research*, vol. 686, pp. 227-233, 2013.
- [9] J. Bell, M. Gordon, and W. Kriven, "Use of geopolymeric cements as a refractory adhesive for metal and ceramic joins," *Ceramic Engineering and Science Proceedings*, vol. 26(3), pp. 407-413, 2005.
- [10] S. Hanjitsuwan, T. Phoo-ngernkham, and N. Damrongwiriyanupap, "Comparative study using Portland cement and calcium carbide residue as a promoter in bottom ash geopolymer mortar," *Construction and Building Materials*, vol. 133, pp. 128-134, 2017.
- [11] L. K. Turner, and F. G. Collins, "Carbon dioxide equivalent (CO₂-e) emissions: A comparison between geopolymer and OPC cement concrete," *Construction and Building Materials*, vol. 43, pp. 125-130, 2013.
- [12] M. L. Kumar, and V. Revathi, "Microstructural properties of alkali-activated metakaolin and bottom ash geopolymer," *Arabian Journal of Science and Engineering* vol. 45, pp. 4235-4246, 2020.
- [13] P. Chindaprasirt, P. De Silva, and S. Hanjitsuwan, "Effect of high-speed mixing on properties of high calcium fly ash geopolymer paste," *Arabian Journal of Science and Engineering*, vol. 39, pp. 6001-6007, 2014.
- [14] G. Mallikarjuna Rao, and T. D. Gunneswara Rao, "Final setting time and compressive strength of fly ash and ggbs-based geopolymer paste and mortar," *Arabian Journal of Science and Engineering*, vol. 40, pp. 3067-3074, 2015.
- [15] A. K. Mandal, and O. P. Sinha, "Effect of bottom ash fineness on properties of red mud geopolymer," *The Journal of Solid Waste Technology and Management*, vol. 43(1), pp. 26-35, 2017.
- [16] J. Davidovits, "Geopolymers based on natural and synthetic metakaolin a critical review," in *the 41st International Conference on Advanced Ceramics and Composites: Ceramic Engineering and Science Proceedings*, vol. 38(3), pp. 201, 2018.
- [17] V. Sata, A. Sathonsaowaphak, and P. Chindaprasirt, "Resistance of lignite bottom ash geopolymer mortar to sulfate and sulfuric acid attack," *Cement and Concrete Composites*, vol. 34, pp. 700-708, 2012.
- [18] R. K. Paramguru, P. C. Rath, and V. N. Mishra, "Trends in red mud utilization – A review," *Mineral Processing and Extractive Metallurgy Review*, vol. 26(1), pp. 1-29, 2004.
- [19] AluminiumInsider. (6 March, 2018). Creating value out of aluminium waste in India, 2017. Available: <https://aluminiuminsider.com/creating-value-aluminium-waste-india/>
- [20] S. Kumar, R. Kumar, and A. Bandopadhyay, "Innovative methodologies for the utilisation of wastes from metallurgical and allied industries," *Resources Conservation and Recycling*, vol. 48, pp. 301-314, 2006.

- [21] B. K. Mahapatra, M. B. S. Rao, R. Bhima Rao, and A. K. Paul, "Characteristics of red mud generated at NALCO refinery, Damanjodi, India, *Light Metals (Warrendale, Pa)*, 2000, pp. 161-170.
- [22] C. R. Borra, B. Blanpain, Y. Pontikes, K. Binnemans, and T. Van Gerven, "Recovery of rare earths and other valuable metals from bauxite residue (red mud): A review," *Journal of Sustainable Metallurgy*, vol. 2, pp. 365-386, 2016.
- [23] T. Hertel, and Y. Pontikes, "Geopolymers, inorganic polymers, alkali-activated materials and hybrid binders from bauxite residue (red mud) – Putting things in perspective," *Journal of Cleaner Production*, vol. 258(10), pp. 120610, 2020.
- [24] A. K. Mandal, H. R. Verma, and O. P. Sinha, "Utilization of aluminum plant's waste for production of insulation bricks," *Journal of Cleaner Production*, vol. 162, pp. 949-957, 2017.
- [25] A. Rai, A. K. Mandal, K. K. Singh, and T. R. Mankhand, "Preparation and characterization of lime activated unfired bricks made with industrial wastes," *International Journal of Waste Resources (IJWR)*, vol. 3, pp. 40-46, 2013.
- [26] S. Samal, A. K. Ray, and A. Bandopadhyay, "Proposal for resources, utilization and processes of red mud in India — A review," *International Journal of Mineral Processing*, vol. 118, pp. 43-55, 2013.
- [27] V. Ajay, C. Rajeev, and R. K. Yadav, "Effect of micro silica on the strength of concrete with ordinary portland cement," *Research Journal of Engineering Sciences*, vol. 1(3), pp. 1-4, 2012.
- [28] F. N. Okoye, J. Durgaprasad, and N. B. Singh, "Effect of silica fume on the mechanical properties of fly ash based-geopolymer concrete," *Ceramic International*, vol. 42, pp. 3000-3006, 2016.
- [29] J. Schaliq, "High-quality sands for calcium-silicate brick production," *Aufbereit Tech*, vol. 37, pp. 368-372, 1996.
- [30] A. Kumar, and S. Kumar, "Development of paving blocks from synergistic use of red mud and fly ash using geopolymerization," *Construction and Building Materials*, vol. 38, pp. 865-871, 2013.
- [31] S. N. M. Hairi, G. N. L. Jameson, J. J. Rogers, and K. J. D. MacKenzie, "Synthesis and properties of inorganic polymers (geopolymers) derived from Bayer process residue (red mud) and bauxite," *Journal of Materials Science*, vol. 50(23), pp. 7713-7724, 2015.
- [32] J. He, Y. Jie, J. Zhang, Y. Yu, and G. Zhang, "Properties of chemically combusted calcium carbide residue and its influence on cement properties," *Materials (Basel)*, vol. 37, pp. 108-118, 2013.
- [33] J. V. N. Raju, T. C. Rao, and V. Ravindra, "An experimental study on fly ash-based geopolymer concrete," *Engineering Sciences International Research Journal*, vol. 1, pp. 108-112, 2013.
- [34] X. Ke, S. A. Bernal, N. Ye, J. L. Provis, and J. Yang, "One-part geopolymers based on thermally treated red mud/NaOH blends," *Journal of the American Ceramic Society*, vol. 98(1), pp. 5-11, 2015.
- [35] L. P. Ogorodova, L. V. Mel'chakova, M. F. Vigasina, L. V. Olyshich, and I. V. Pekov, "Cancrinite and cancrisilite in the Khibina-Lovozero alkaline complex: Thermochemical and thermal data," *Geochemistry International*, vol. 47(3), pp. 260-267, 2009.
- [36] R. N. Thakur, and S. Ghosh, "Effect of mix composition on compressive strength and microstructure of fly ash based geopolymer composites," *Journal of Engineering and Applied Sciences*, vol. 4(4), pp. 68-74, 2009.
- [37] J. N. Y. Djobo, A. Elimbi, H. K. Tchakouté, and S. Kumar, "Mechanical activation of volcanic ash for geopolymer synthesis: effect on reaction kinetics, gel characteristics, physical and mechanical properties," *RSC Advances*, vol. 6(45), pp. 39106-39117, 2016.
- [38] S. Alonso, and A. Palomo, "Alkaline activation of metakaolin and calcium hydroxide mixtures: Influence of temperature, activator concentration and solids ratio," *Materials Letters*, vol. 47(1-2), pp. 55-62, 2001.
- [39] D. Khale, and R. Chaudhary, "Mechanism of geopolymerization and factors influencing its development: A review," *Journal of Materials Science*, vol. 42(3), pp. 729-746, 2007.
- [40] D. Taylor, "Strength-component size relationship for high-tension insulator whiteware," *British Ceramic Transactions*, vol. 88(6), pp. 209-212, 1989.
- [41] J. Davidovits, M. Davidovics, and N. Davidovits, "Process for obtaining a geopolymeric aluminosilicate and products thus obtained," U.S. Patent 5,342,595, August 30, 1994.
- [42] V. F. F. Barbosa, K. J. D. MacKenzie, and C. Thaumaturgo, "Synthesis and characterisation of materials based on inorganic polymers of alumina and silica: Sodium polysialate polymers," *International Journal of Inorganic Materials*, vol. 2(4), pp. 309-317, 2000.
- [43] K. Boonserm, V. Sata, K. Pimraksa, and P. Chindaprasirt, "Improved geopolymerization of bottom ash by incorporating fly ash and using waste gypsum as additive," *Cement and Concrete Composite*, vol. 34(7), pp. 819-824, 2012.
- [44] Y. Fang, Y. Gu, Q. Kang, Q. Wen, and P. Dai, "Utilization of copper tailing for autoclaved sand – lime brick," *Constructure and Building Materials*, vol. 25(25), pp. 867-872, 2011.
- [45] C. Shi, and R. L. Day, "Pozzolanic reaction in the presence of chemical activators: Part II — Reaction products and mechanism," *Cement and Concrete Research*, vol. 30(4), pp. 607-613, 2000.
- [46] A. K. Mandal, "Production of lime-stabilized thermal insulation bricks using aluminum mine tailing," *Journal of The Institution of Engineers (India): Series A*, vol. 102(1), pp. 249-258, 2021.
- [47] S. Prasanphan, A. Wannagon, T. Kobayashi, and S. Jiemsirilars, "Microstructure evolution and mechanical properties of calcined kaolin processing waste-based geopolymers in the presence of different alkali activator content by pressing and casting", *Journal of Metals, Materials and Minerals*, vol. 30(3), pp. 121-132, 2020.
- [48] P. N. Lemougna, K. J. D. MacKenzie, G. N. L. Jameson, H. Rahier, and U. F. Chinje Melo, "The role of iron in the formation of inorganic polymers (geopolymers) from volcanic ash: A ⁵⁷Fe Mössbauer spectroscopy study," *Journal of Materials Science*, vol. 48(15), pp. 5280-5286, 2013.
- [49] P. Duxson, A. Fernández-Jiménez, J. L. Provis, G. C. Lukey, A. Palomo, and J. S. J. van Deventer, "Geopolymer technology: the current state of the art," *Journal of Materials Science*, vol. 42(9), pp. 2917-2933, 2007.

- [50] H. K. Kim, J. H. Jeon, and H. K. Lee, "Flow, water absorption, and mechanical characteristics of normal- and high-strength mortar incorporating fine bottom ash aggregates," *Constructure and Building Materials*, vol. 26(1), pp. 249-256, 2012.
- [51] S. K. Amin, S. A. El-Sherbiny, A. A. M. A. El-Magd, A. Belal, and M. F. Abadir, "Fabrication of geopolymer bricks using ceramic dust waste," *Constructure and Building Materials*, vol. 157, pp.610-620, 2017.
- [52] Y. M. Liew, H. Kamarudin, A. M. Mustafa Al Bakri, M. Bnhussain, M. Luqman, I. Khairul Nizar, C. M. Ruzaidi, and C. Y. Heah, "Optimization of solids-to-liquid and alkali activator ratios of calcined kaolin geopolymeric powder," *Constructure and Building Materials*, vol. 37, pp. 440-451, 2012.